Broad Line Region

Introduction

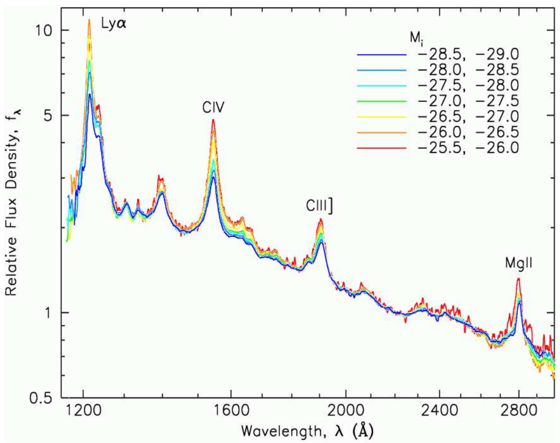

Average quasar spectra for $2.03 < z < 2.311$, normalized to the same flux at $\lambda = 2200$Å (vanden Berk et al., 2004, Fig. 1)

Review: Peterson (2006)

- Overall, spectral *shape* is luminosity independent
- Baldwin effect: Emission lines (esp. Lyα and C IV 1549Å) weaker in more luminous objects, although shape similar.

This chapter: physics of region emitting the broad lines.

Properties

General properties of the BLR from observed spectrum:

- Emission lines from BLR: typical for $T \sim 10^4$ K (photoionization)
- Lines have widths of 500...25000 km s^{-1}

  Thermal motion:
  $$E_{\text{kin}} = \frac{1}{2} m_{\text{p}} v^2 = \frac{3}{2} kT \tag{8.1}$$
  $\Longrightarrow$ Typical thermal speed:
  $$v \sim \sqrt{\frac{3kT}{m_{\text{p}}}} \sim 20\,\text{km}\,\text{s}^{-1} \tag{8.2}$$
- Line broadening is due to supersonic bulk motion of BLR emitting gas
- No [O III] 4959/5007 lines $\Longrightarrow n \gtrsim n_{\text{crit, 5077}} \sim 10^8\,\text{cm}^{-3}$.
- C iii] 1909 line sometimes broad, so $n \lesssim n_{\text{crit, 1909}} \sim 10^{10}\,\text{cm}^{-3}$.

  More detailed analyses show C iii] to originate in region different from Lyα emitting region, typical densities can be as high as $10^{11}\,\text{cm}^{-3}$.

Location

Location of BLR from line width:

Assume emitting gas on a circular orbit:

Kepler speed:
$$\frac{mv^2}{r} = \frac{GMm}{r^2} \quad \Longrightarrow \quad v = \sqrt{\frac{GM}{r}} \tag{8.3}$$
such that
$$r = \frac{GM}{v^2} = 3600\,\text{AU} \left(\frac{M}{10^6\,M_\odot}\right) \left(\frac{v}{500\,\text{km}\,\text{s}^{-1}}\right)^{-2} \tag{8.4}$$

The BLR is located close to the central black hole.

Note: BLR probably does *not* consist of gas on circular orbits around the BH, so real size is larger.

BLR: Mass

Mass determination: Determine number of emitting atoms from line strength, e.g., Hβ (less influenced by radiative transfer effects than Lyman lines)

Line emissivity:

$$j_{\mathrm{H}\beta} = n_{\mathrm{e}} n_{\mathrm{p}} \alpha_{\mathrm{H}\beta} \frac{h\nu_{\mathrm{H}\beta}}{4\pi} = n_{\mathrm{e}}^2 \alpha_{\mathrm{H}\beta}^{\mathrm{eff}} \frac{h\nu_{\mathrm{H}\beta}}{4\pi} = 1.24 \times 10^{-25}\,\mathrm{erg\,s^{-1}\,cm^{-3}\,sr^{-1}} \frac{n_{\mathrm{e}}^2}{4\pi} \qquad (8.5)$$

where $\alpha_{\mathrm{H}\beta}^{\mathrm{eff}}$: effective recombination coefficient for $n = 4 \to n = 2$ transition (weakly temperature dependent).

Total Hβ luminosity:

$$L_{\mathrm{H}\beta} = \iint j_{\mathrm{H}\beta}\, \mathrm{d}\Omega\, \mathrm{d}V = \frac{4\pi n_{\mathrm{e}}^2}{3} \cdot 1.24 \times 10^{-25} r^3 f\, \mathrm{erg\,s^{-1}} \propto \int n_{\mathrm{e}}^2 \mathrm{d}V \qquad (8.6)$$

where $\int n_{\mathrm{e}}^2 \mathrm{d}V$: emission measure, and f: filling factor.

BLR lines give BLR mass of $\sim$1 $M_\odot$ and $f \sim 10^{-3}$.

Observed lines are bright because of n^2-proportionality and high density of BLR gas.

BLR Line Variability

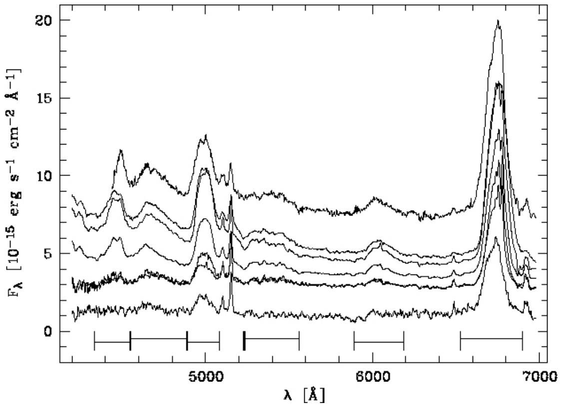

Spectral variability of NGC 7603 (Sy 1), top to bottom: Dec 98, Dec 93, Sep 93, Aug 92, Jul 90, Oct 88, and Oct 79 (Kollatschny, Bischoff & Dietrich, 2000, Fig. 2)

Broad lines are variable on timescales from days to years.

BLR Line Variability

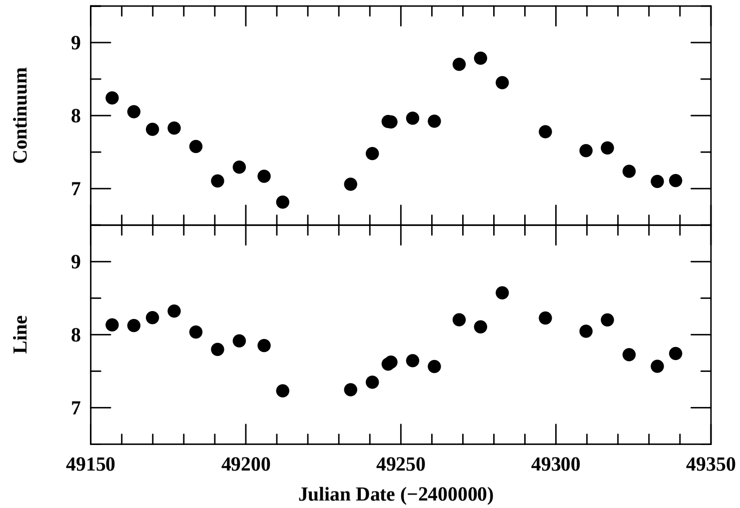

Continuum and Hβ fluxes for Mkn 335 (Peterson, 2001, Fig. 23)

BLR Line Variability

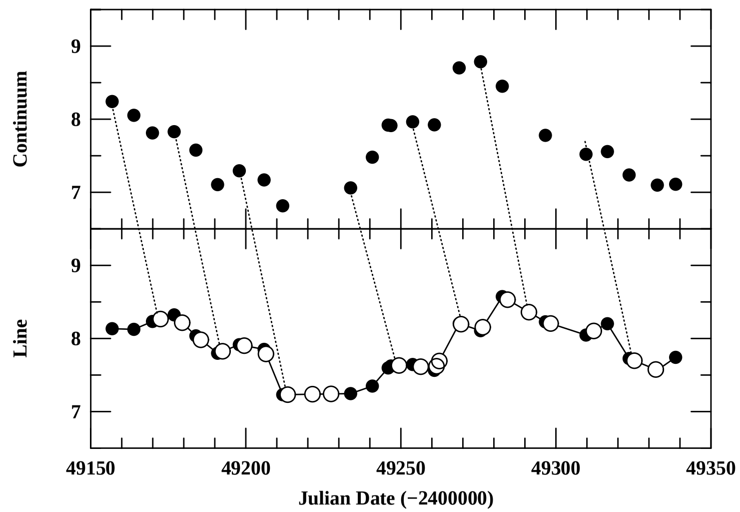

Mkn 335: Hβ line lags continuum by 15.6 d (Peterson, 2001, Fig. 24)

Reverberation Mapping

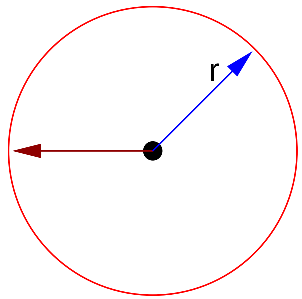

AGN time variability helps to map gas around Black Hole.

Flash at time $t = 0$ will illuminate gas at distance r after time delay

$$\tau = r/c \qquad (8.7)$$

Gas is ionized by flash. Recombination timescale of gas is

$$\tilde{\tau} = \frac{1}{n_e \alpha} \sim 40 n_{11}^{-1}\,\text{s} \qquad (8.8)$$

i.e., “quasi instantaneous”.

Reverberation Mapping

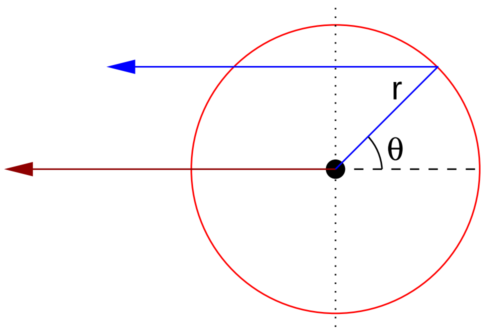

Light emitted by illuminated gas will be observed only after a time delay.
Extra distance traveled by light from r:

$$r' = r + r\cos\theta \qquad (8.9)$$

Time delay due to light travel effect:

$$\tau = (1+\cos\theta)\frac{r}{c} \qquad (8.10)$$

Reverberation Mapping

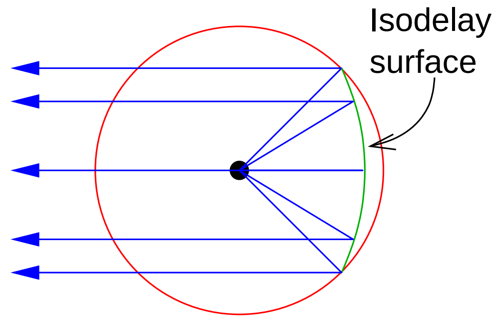

Time delay was given by:

$$\tau = (1+\cos\theta)\frac{r}{c} \qquad (8.10)$$

Locus of points with same time delay (isodelay surface):

$$r(\tau) = \frac{c\tau}{1+\cos\theta} \qquad (8.11)$$

(i.e., a parabola)

Reverberation Mapping

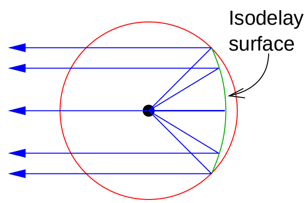

Assume that line intensity increases by factor ζ when BLR gas is illuminated by flash.
$\Longrightarrow$ total line emissivity increase from the isodelay surface:

$$\Psi(\theta)d\theta = \zeta \cdot 2\pi r^2 \sin\theta\, d\theta \qquad (8.12)$$

This assumes that conditions in BLR at r are the same everywhere.

$\Psi(r)d\theta$ corresponds to a response at time delay τ:

$$\Psi(\tau)d\tau = \Psi(\theta)d\theta \left|\frac{d\theta}{d\tau}\right| d\tau = \zeta \cdot 2\pi r^2 \sin\theta \cdot \frac{c}{r\sin\theta} d\tau = 2\pi\zeta r c\, d\tau \qquad (8.13)$$

where $\tau = (1+\cos\theta)r/c$, i.e., $d\tau/d\theta = -\sin\theta \cdot r/c$ was used.

Reverberation Mapping

In reality, AGN does not emit shots, but nucleus varies stochastically

$\Longrightarrow$ Reverberation mapping (Blandford & McKee, 1982)

Describe continuum variability as $C(t)$.

Observed line variability, L, is:

$$L(t) = \int_{-\infty}^{+\infty} \Psi(\tau) C(t-\tau) d\tau \tag{8.14}$$

("convolution" of C with kernel $\Psi(\tau)$).

Observational problem is the inverse of Eq. (8.14): Given $L(t)$, determine $\Psi(\tau)$.

- . . . provided the lightcurve is long enough, as τ can be days to months!
- $C(t-\tau)$ is known from continuum variations

Reverberation Mapping

To solve equations such as

$$L(t) = \int_{-\infty}^{+\infty} \Psi(\tau) C(t-\tau) d\tau \tag{8.14}$$

for Ψ, the standard approach in mathematics is to determine the Fourier transform of $L(t)$:

$$L(f) = \int_{-\infty}^{+\infty} L(t) e^{-2\pi i f t}\, dt \tag{8.15}$$

inserting Eq. (8.14) gives

$$= \int_{-\infty}^{+\infty} \int_{-\infty}^{+\infty} \Psi(\tau) C(t-\tau) e^{-2\pi i f t}\, d\tau\, dt \tag{8.16}$$

change order of integration

$$= \int_{-\infty}^{+\infty} \Psi(\tau) \int_{-\infty}^{+\infty} C(t-\tau) e^{-2\pi i f t}\, dt\, d\tau \tag{8.17}$$

substitute $t - \tau \longrightarrow t'$

$$= \int_{-\infty}^{+\infty} \Psi(\tau) \int_{-\infty}^{+\infty} C(t') e^{-2\pi i f (t'+\tau)}\, dt'\, d\tau \tag{8.18}$$

Reverberation Mapping

Therefore

$$L(f) = \int_{-\infty}^{+\infty} \Psi(\tau) \int_{-\infty}^{+\infty} C(t') e^{-2\pi i f (t'+\tau)}\, dt'\, d\tau \tag{8.18}$$

move constant outside of the inner integral and drop the prime

$$= \int_{-\infty}^{+\infty} \Psi(\tau) e^{-2\pi i f \tau} \int_{-\infty}^{+\infty} C(t) e^{-2\pi i f t}\, dt\, d\tau \tag{8.19}$$

since the inner integral is a constant this gives

$$= \int_{-\infty}^{+\infty} e^{-2\pi i f \tau} \Psi(\tau) d\tau \cdot \int_{-\infty}^{+\infty} C(t) e^{-2\pi i f t} dt \tag{8.20}$$

which is the product of the Fourier transforms of C and Ψ:

$$L(f) = \Psi(f) \cdot C(f) \tag{8.21}$$

The Fourier transform of L is the product of the Fourier transforms of Ψ and C.

This is just the convolution theorem of Fourier theory.

Reverberation Mapping

Blandford & McKee (1982): Since $L(f)$ and $C(f)$ can be measured, we can determine $\Psi(f)$ and then do an inverse FT:

$$\Psi(t) = \frac{1}{2\pi} \int_{-\infty}^{+\infty} \Psi(f) e^{+2\pi i f t} df \tag{8.22}$$

so we can in principle measure $\Psi(f)$.

In practice: Fourier approach does not work.

Reason: Sparse sampling of lightcurves

$\Longrightarrow$ Potential of reverberation mapping has not yet been realized!

What *is* possible is to determine size of BLR from reverberation mapping

Reverberation Mapping

To get BLR size from reverberation, work in time domain and determine cross correlation of $L(t)$ and $C(t)$:

$$\mathrm{CCF}(\tau) = \int_{-\infty}^{+\infty} L(t)C(t-\tau)dt \tag{8.23}$$

insert $L(t)$ from Eq. (8.14):

$$= \int_{-\infty}^{+\infty} C(t-\tau) \int_{-\infty}^{+\infty} C(t-\tau')\Psi(\tau')d\tau'\,dt \tag{8.24}$$

change order of integration

$$= \int_{-\infty}^{+\infty} \Psi(\tau') \int_{-\infty}^{+\infty} C(t-\tau)C(t-\tau')dt\,d\tau' \tag{8.25}$$

and introduce the auto correlation function, ACF,

$$= \int_{-\infty}^{+\infty} \Psi(\tau')\mathrm{ACF}(\tau-\tau')d\tau' \tag{8.26}$$

where

$$\mathrm{ACF}(\tau) = \int_{-\infty}^{+\infty} C(t)C(t-\tau)dt \tag{8.27}$$

Reverberation Mapping

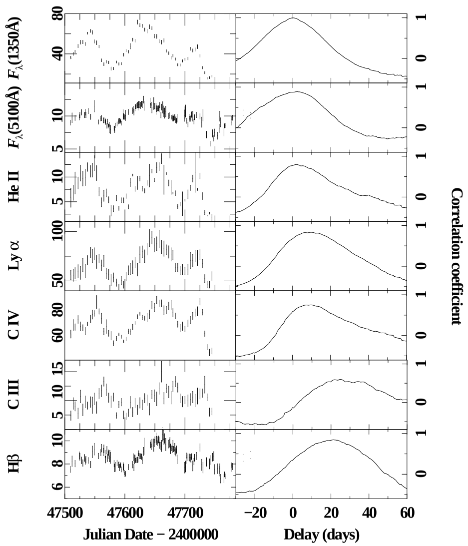

CCF has a peak at the lag for which $C(t)$ and $L(t)$ match best
$\Longrightarrow$ Based on the CCF we can measure the size of the BLR.

In practice, one has to interpolate $C(t)$ and $L(t)$ to determine CCF using a discretized version of the integrals shown previously.

Light curves and CCFs with respect to 1350Å UV continuum for NGC 5548 (Clavel et al., 1992; Peterson, 2001).

Reverberation Mapping

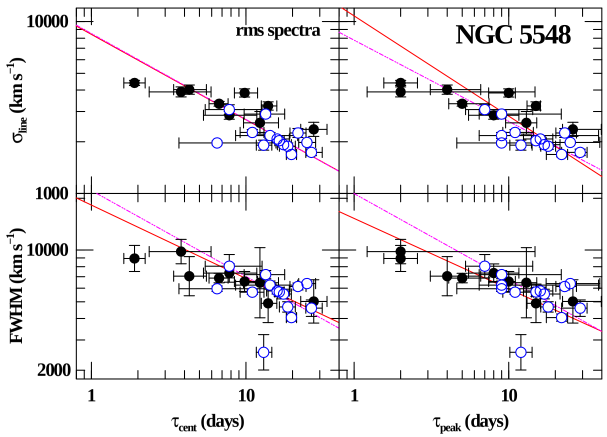

(Peterson et al., 2004, Fig. 3)

As expected: broadest lines vary fastest.

Also found: higher ionization lines vary fastest $\Longrightarrow$ BLR has a stratified ionization structure

Reverberation Mapping

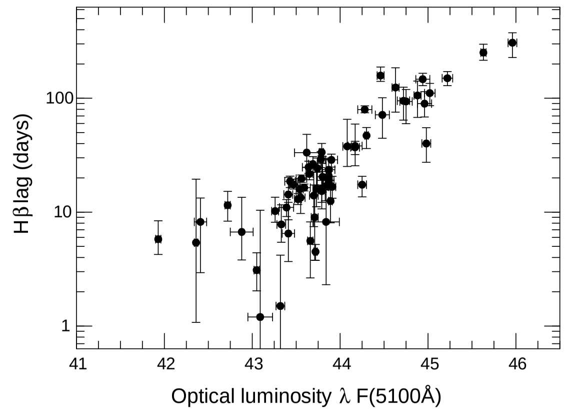

(Peterson, 2006, Fig. 6)

The photoionization parameter is $U \propto L/(D^2 n_e)$ (Eq. 7.20) so for U, n_e constant, we expect $D \propto L^{0.5}$. This is roughly what is observed!

U = const. is expected since AGN spectra are all similar, so conditions in BLR are similar everywhere ("locally optimally emitting clouds").

Reverberation Mapping

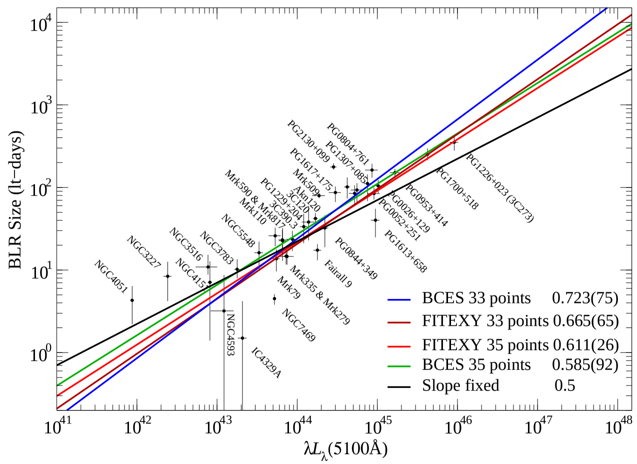

(Kaspi et al., 2005, Fig. 2)

In detail, things are more complicated, and slope is steeper than 0.5: $R \propto L^{0.67\pm0.05}$

$\Longrightarrow$ ionization parameter, density, and spectral shape depend somewhat on L.

What is the BLR?

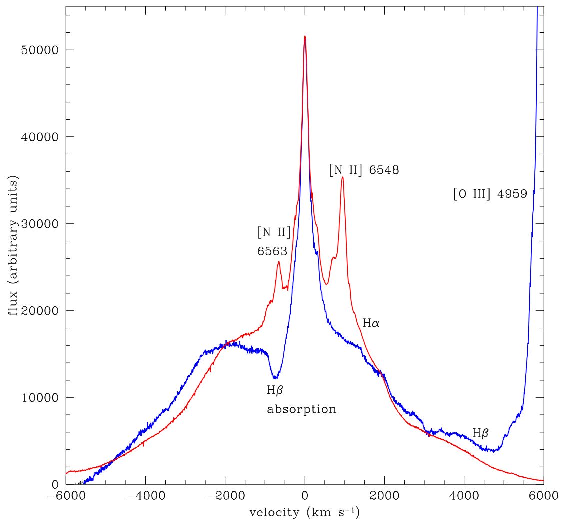

NGC 4151 (Sy 1; Arav et al., 1998, Fig. 1)

Classical assumption: BLR is collection of cold clouds embedded in hot gas

("two phase medium", Krolik, McKee & Tarter 1981)

$\Longrightarrow$ We expect to see evidence for emission from individual clouds.

Problem: BLR line profiles are *always* smooth!

$\Longrightarrow$ Does the BLR consist of *many* small clouds?

What is the BLR?

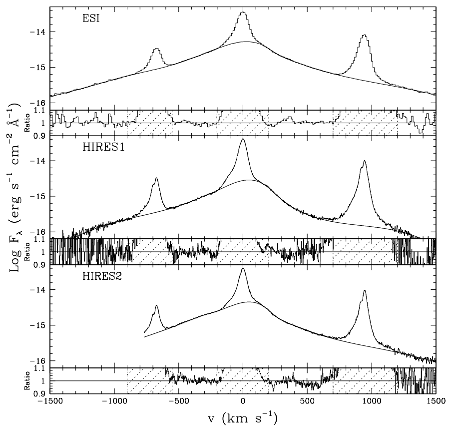

(NGC 4395 Laor et al., 2006)

Observations show always smooth BLR profiles, even for lowest luminosity AGN such as NGC 4395 (the lowest luminosity Sy 1 known)

$\Longrightarrow$ this is only possible if there is a *very large* number of clouds such that it is better to speak about a "clumpy" gas.

For NGC 4151, Arav et al. (1998) find that there must be $\gtrsim 3 \times 10^7$ clouds, for NGC 4395, $> 10^5$ clouds are required (Laor et al., 2006). Since $R_{\text{BLR, 4395}} \sim 10^{14}$ cm from reverberation, $R_{\text{cloud, 4395}} \lesssim 10^{12}$ cm, i.e., much smaller than stars.

The BLR cannot consist of individual clouds, it rather is a smooth(ish) gas cloud surrounding the BH.

What is the BLR?

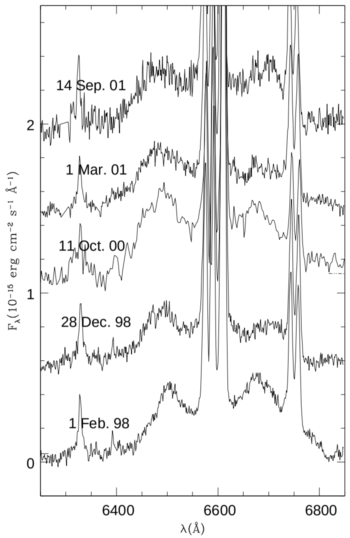

In some AGN BLR profiles are double humped

NGC 1097 (Sy1; Storchi-Bergmann et al., 2003, Fig. 8)

What is the BLR?

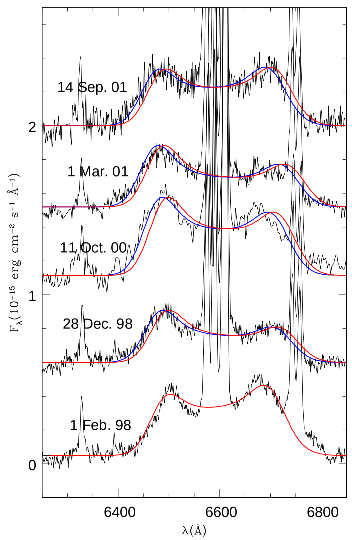

In some AGN BLR profiles are double humped
⟹ is BLR the outer edge of accretion disk?

NGC 1097 (Sy1; Storchi-Bergmann et al., 2003, Fig. 8)

Winds

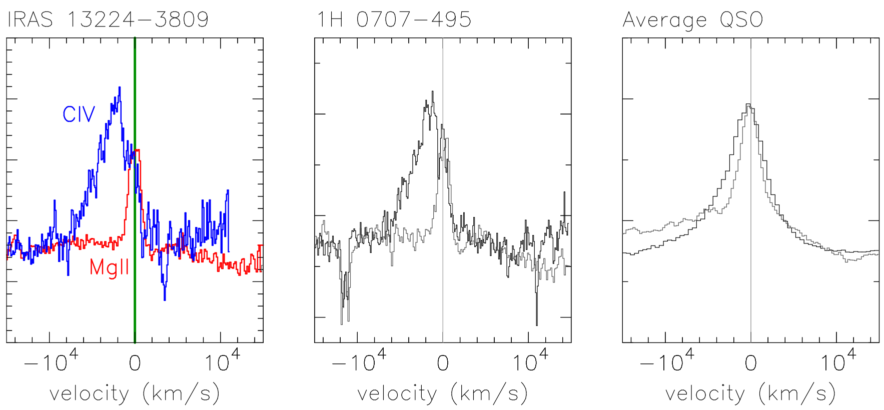

(Leighly & Moore, 2004)

While disk emission explains part of BLR emission, not all features can be explained: Sy 1 show asymmetric line profiles: Higher ionization lines are shifted bluewards ⟹ Outflow!

Winds

There are also findings that the line blueshift increases with AGN luminosity: evidence for radiatively driven outflows?

Is the BLR an accretion disk wind?

Driving mechanisms:

- Electromagnetic?
  related to jet?
- Radiatively driven?
  related to high AGN luminosity

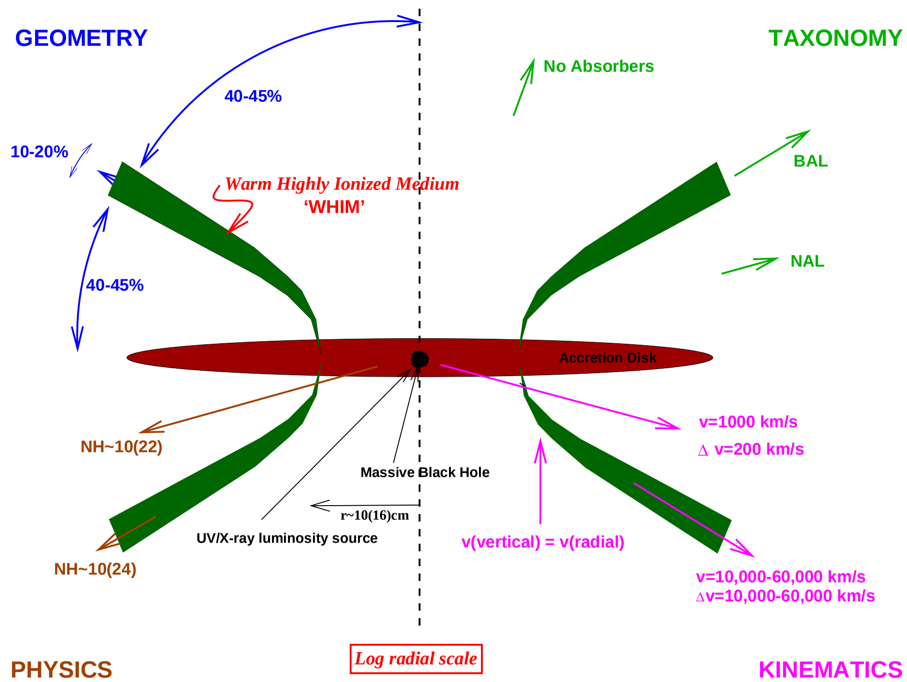

(Elvis, 2000, Fig. 1)

8–28

BH Masses

Regardless of the detailed interpretation of the BLR, measurements of the BLR allow for a (statistical) determination of the mass of the Black Hole:

The virial theorem of mechanics states:

$$2T = m\Delta V^2 = \eta \cdot G\frac{mM_{\rm BH}}{r_0} = U \qquad (8.28)$$

where m mass of a test particle, r_0: characteristic BLR radius, ΔV: velocity dispersion, and η: geometry dependent factor.

Since r_0 and ΔV can be measured from reverberation mapping and the line width:

$$M_{\rm BH} = f \cdot \frac{r\Delta V^2}{G} \qquad (8.29)$$

where f is a geometry dependent normalization factor, obtained from calibration measurements.

Note: For virial theorem to apply, motion of BLR must be dominated by gravity.

8–28

To derive the virial theorem, we look at a system of particles of mass m_i. The acceleration on particle i by all other particles is

$$\ddot{\mathbf{r}} = \sum_{j\neq i} \frac{Gm_j(\mathbf{r}_j - \mathbf{r}_i)}{|\mathbf{r}_j - \mathbf{r}_i|^3} \qquad (8.30)$$

…scalar product with $m_i\mathbf{r}_i$

$$m_i\mathbf{r}_i \cdot \ddot{\mathbf{r}}_i = \sum_{j\neq i} \frac{Gm_im_j\mathbf{r}_i \cdot (\mathbf{r}_j - \mathbf{r}_i)}{|\mathbf{r}_j - \mathbf{r}_i|^3} \qquad (8.31)$$

…since

$$\frac{1}{2}\frac{d^2\mathbf{r}_i^2}{dt^2} = \frac{d}{dt}(\dot{\mathbf{r}}_i \cdot \mathbf{r}_i) = \ddot{\mathbf{r}}_i \cdot \mathbf{r}_i + \dot{\mathbf{r}}_i \cdot \mathbf{r}_i \qquad (8.32)$$

…therefore Eq. (8.31)

$$\frac{1}{2}\frac{d^2}{dt^2}(m_i\mathbf{r}_i^2) - m_i\dot{\mathbf{r}}_i{}^2 = \sum_{j\neq i} \frac{Gm_im_j\mathbf{r}_i \cdot (\mathbf{r}_j - \mathbf{r}_i)}{|\mathbf{r}_j - \mathbf{r}_i|^3} \qquad (8.33)$$

Summing over all particles in the system gives

$$\frac{1}{2}\sum_i \frac{d^2}{dt^2}(m_i\mathbf{r}_i^2) - \sum_i m_i\dot{\mathbf{r}}_i{}^2 = \sum_i\sum_{j\neq i} \frac{Gm_im_j\mathbf{r}_i \cdot (\mathbf{r}_j - \mathbf{r}_i)}{|\mathbf{r}_j - \mathbf{r}_i|^3} \qquad (8.34)$$

$$= \frac{1}{2}\left(\sum_i\sum_{j\neq i} Gm_im_j \frac{\mathbf{r}_i \cdot (\mathbf{r}_j - \mathbf{r}_i)}{|\mathbf{r}_i - \mathbf{r}_j|^3} + \sum_j\sum_{i\neq j} Gm_jm_i \frac{\mathbf{r}_j \cdot (\mathbf{r}_i - \mathbf{r}_j)}{|\mathbf{r}_j - \mathbf{r}_i|^3}\right) \qquad (8.35)$$

$$= \frac{1}{2}\left(\sum_i\sum_{j\neq i} Gm_im_j \frac{\mathbf{r}_i \cdot \mathbf{r}_j - \mathbf{r}_i^2}{|\mathbf{r}_i - \mathbf{r}_j|^3} + \sum_j\sum_{i\neq j} Gm_jm_i \frac{\mathbf{r}_j \cdot \mathbf{r}_i - \mathbf{r}_j^2}{|\mathbf{r}_j - \mathbf{r}_i|^3}\right) \qquad (8.36)$$

$$= -\frac{1}{2}\sum_{\substack{i,j\\ i\neq j}} \frac{Gm_im_j}{|\mathbf{r}_i - \mathbf{r}_j|} \qquad (8.37)$$

8–28

Thus, identifying the total kinetic energy, T, and the gravitational potential energy, U, gives

$$2T - U = \frac{1}{2}\frac{d^2}{dt^2}\sum_i m_i\mathbf{r}_i^2 = 0 \qquad (8.38)$$

in statistical equilibrium.

Thus we find the virial theorem: $T = \frac{1}{2}|U|$

8–29

BH Masses

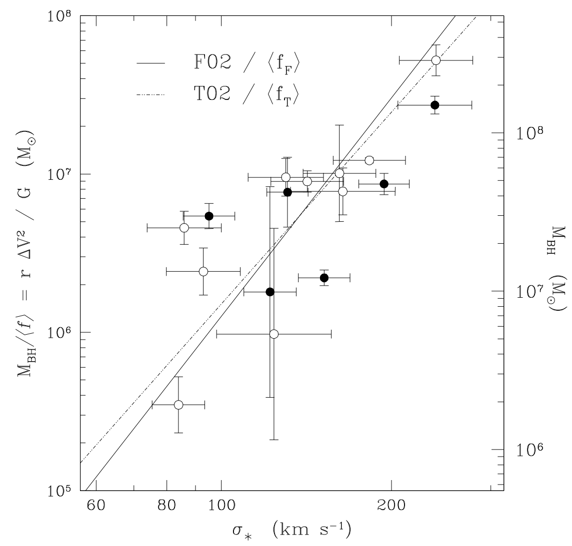

Onken et al. (2004): Calibration of reverberation mapping based on other AGN mass determinations (M–σ-relationship, see later):

$$f = 5.5 \pm 1.9$$

$\Longrightarrow$ Masses determined from reverberation mapping are exact to ~35%.

BH Masses

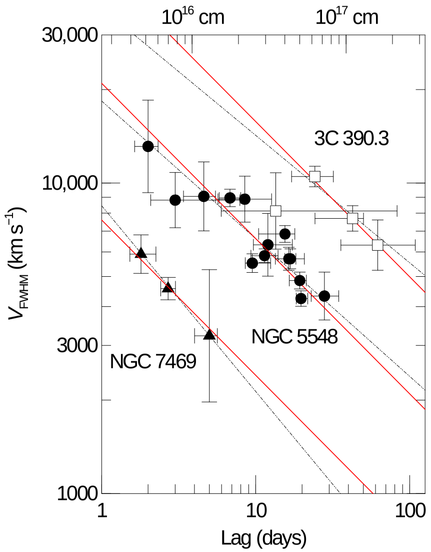

Since $M \propto r\Delta V^2$, for a single object (M = const.), we expect $r \propto \Delta V^{-1/2}$.

Observations: Line width versus lag scales as

$$\log V_{\text{rms}} = a + b \log c\tau \quad (8.39)$$

with $b = -1/2$, as expected!

solid lines in the figure

Masses obtained from lag and V (Peterson & Wandel, 2000):

- NGC 7469: 8.4 × 10^6 $M_\odot$
- NGC 5548: 5.9 × 10^7 $M_\odot$
- 3C 390.3: 3.2 × 10^8 $M_\odot$

(Peterson, 2001)

Arav, N., Barlow, T. A., Laor, A., Sargent, W. L. W., & Blandford, R. D., 1998, MNRAS, 297, 990

Blandford, R. D., & McKee, C. F., 1982, ApJ, 255, 419

Clavel, J., et al., 1992, ApJ, 393, 113

Elvis, M., 2000, ApJ, 545, 63

Kaspi, S., Maoz, D., Netzer, H., Peterson, B. M., Vestergaard, M., & Jannuzi, B. T., 2005, ApJ, 629, 61

Kollatschny, W., Bischoff, K., & Dietrich, M., 2000, A&A, 361, 901

Krolik, J. H., McKee, C. F., & Tarter, C. B., 1981, ApJ, 249, 422

Laor, A., Barth, A. J., Ho, L. C., & Filippenko, A. V., 2006, ApJ, 636, 83

Leighly, K. M., & Moore, J. R., 2004, ApJ, 611, 107

Onken, C. A., Ferrarese, L., Merritt, D., Peterson, B. M., Pogge, R. W., Vestergaard, M., & Wandel, A., 2004, ApJ, 615, 645

Peterson, B. M., 2001, in Advanced Lectures on the Starburst-AGN Connection, ed. I. Aretxaga, D. Kunth, R. Mújica, (Singapore: World Scientific), 3

Peterson, B. M., 2006, in Physics of Active Galactic Nuclei at All Scales, ed. D. Alloin, R. Johnson, P. Lira, Vol. 693, (Berlin, Heidelberg: Springer), 77

Peterson, B. M., et al., 2004, ApJ, 613, 682

Peterson, B. M., & Wandel, A., 2000, ApJ, 521, L95

Storchi-Bergmann, T., et al., 2003, ApJ, 598, 956

vanden Berk, D., Yip, C., Connolly, A., Jester, S., & Stoughton, C., 2004, in AGN Physics with the Sloan Digital Sky Survey, ed. G. T. Richards, P. B. Hall, 21

BH Masses

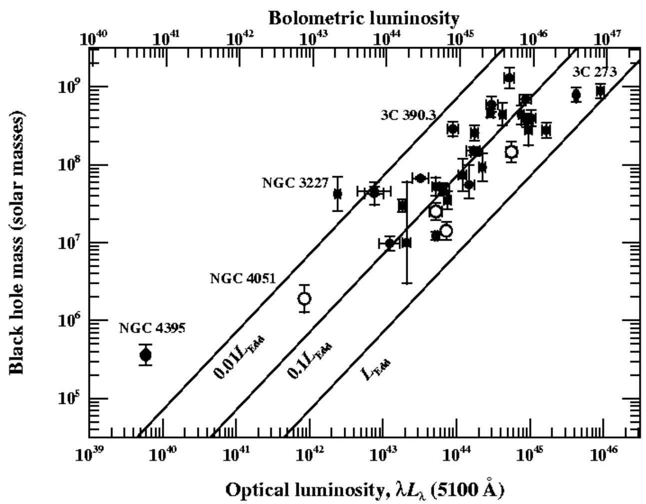

Until today: 36 AGN with reverberation measurements. Mass-luminosity relationship: typical efficiency for AGN accretion is 10%.

Peterson (2006; Xian AGN workshop)

Narrow Line Region

General Properties

Reminder: Narrow Line Region (Osterbrock, 1989, 1991):

- Line widths 200–700 km s^{-1}
- Allowed lines from H I, He I, He II
- Forbidden lines: strongest: [O III] $\lambda\lambda$4959, 5007, [N II] $\lambda\lambda$6548, 6583
- Studies for Sy 1 problematic as narrow and broad lines blend
- Gas diagnostics from [O III] $\lambda\lambda$ 5007/4959 and 4363 and [S II λ6716/λ6731 ratios: $T \sim$ 15000 K and $n_\mathrm{e} \sim 3 \times 10^3\,\mathrm{cm}^{-3}$, possible density gradient is observed
- NLR mass from Hβ emissivity and assuming spherical symmetry: $L_{\mathrm{H}\beta} = 2 \times 10^8\,L_\odot \Longrightarrow M \sim 7 \times 10^5 (10^4/N_\mathrm{e}) M_\odot$ and $R \sim 20 f^{-1/3} (10^4/N_\mathrm{e})^{2/3}$ pc, i.e., 90 pc with an estimated filling factor of $f = 10^{-2}$.

NLR Modeling

Models of the NLR aim to

- Determine flux of lines
- Reproduce line ratios and equivalent widths of narrow lines
- provide estimates for the line width

See talk by B. Groves at Xian AGN meeting for details:
`http://agn06.ihep.ac.cn/`

Nature of the NLR

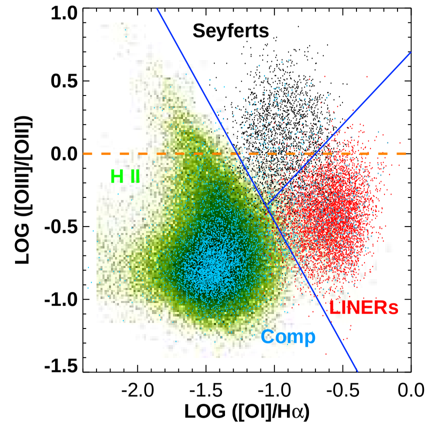

(Kewley et al., 2006)

Reminder: Line ratios are used to define the different types of Seyfert galaxies.

(Kewley et al., 2006; Baldwin, Phillips & Terlevich, 1981)

Nature of the NLR

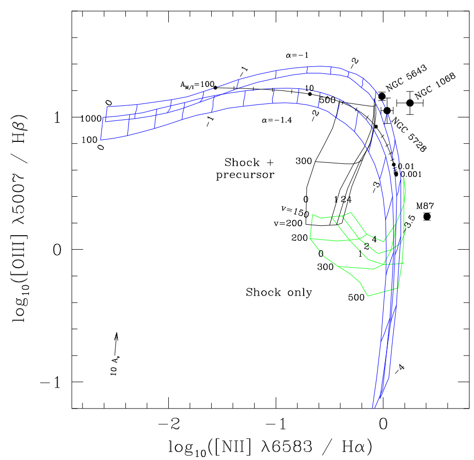

(Allen et al., 1999, Fig. 1)

Photoionization models can reproduce ratios of strong observed lines such as [O III 5007]/Hβ ratio and absolute luminosity of these lines.

BUT: Strengths of high and low ionization stages cannot be reproduced simultaneously!

$\Longrightarrow$ rules out the simplest photoionization models!

Potential solution: shock ionization (Allen et al., 1999, and therein)!

Photons produced after a shock (where $T \sim 10^6$ K) can ionize pre-shock gas $\Longrightarrow$ combination of collisional ionization and photoionization.

Shock possibly related to jet/radio outflow.

Nature of the NLR

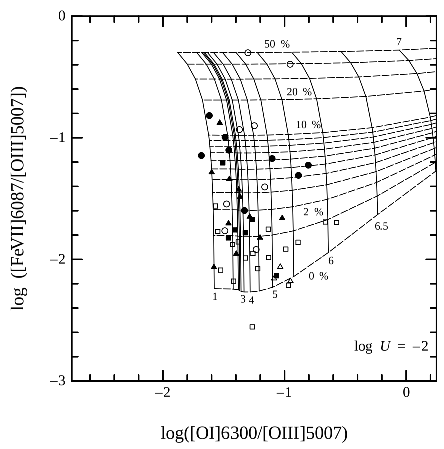

(Murayama & Taniguchi, 1998, Fig. 2)

Alternative explanation of unusual line ratios: two and multiple zone NLR models.

Triggered, e.g., by too strong Fe line emission

For example: High ionization nuclear emission region (HINER) models (Murayama & Taniguchi, 1998): 10% of NLR emission from high density ($n_e \sim 10^9\,\mathrm{cm}^{-3}$) photoionized region within torus which is responsible for emission from high ionized species.

Similar models have also been proposed, e.g, by Komossa & Schulz (1997) and by many other authors.

Problem: Too many free parameters
$\Longrightarrow$ Search for physical constraints!

E.g., matter bounded vs. ionization bounded clouds, locally optimally emitting clouds,. . .

NGC 1068 (M77), NOAO 20″

Francois and Shelley Pelletier/Adam Block/NOAO/AURA/NSF

Imaging of the NLR

Line diagnostics: size of NLR: ∼90 pc or larger.

$\Longrightarrow$ for the nearest AGN imaging is possible

(e.g., Circinus galaxy: $d = 4$ Mpc $\longrightarrow 1'' = 19$ pc.

Imaging of NLR possible either using integral field spectroscopy or narrow-band filters.

Often used: narrow-band Hα and [O III] filters.

Results (see, e.g., Pogge 1988):

- ionization cones,
- stratified ionization structure in many AGN.

$\Longrightarrow$ Extended Narrow Line Region (ENLR).

In the following: two typical examples: NGC 1068 (=M77) and Circinus galaxy.

Similar studies have been performed for $\gtrsim 30$ nearby AGN.

NGC 1068

NGC 1068 (M77) (Bill Arnett)

NGC 1068 (M77): Seyfert 2 nucleus at $z = 0.003$ ($d \sim 15$ Mpc), one of the best studied galaxies in the sky.

NGC 1068

NGC 1068 (M77) core with HST in O III

NGC 1068 (M77): Seyfert 2 nucleus at $z = 0.003$ ($d \sim 15$ Mpc), one of the best studied galaxies in the sky.

Pogge (1988): Extended ionizing radiation cone from the nucleus of NGC 1068, along the direction of the radio jet.

Circinus galaxy:

- $d \sim 4$ Mpc ($1'' \sim 19$ pc)
- 2nd nearest AGN on southern hemisphere after Cen A
- SAb galaxy
- Seyfert 2 nucleus

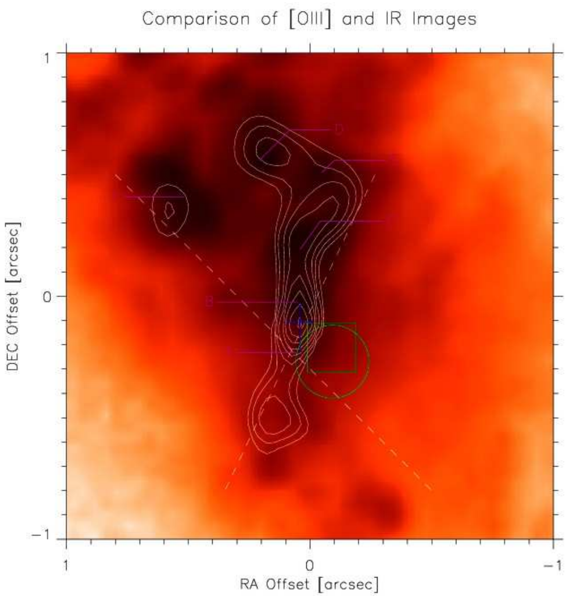

M. Camenzind

NGC 1068: Funnel in IR overlaid to O III image: Highly structured NLR!

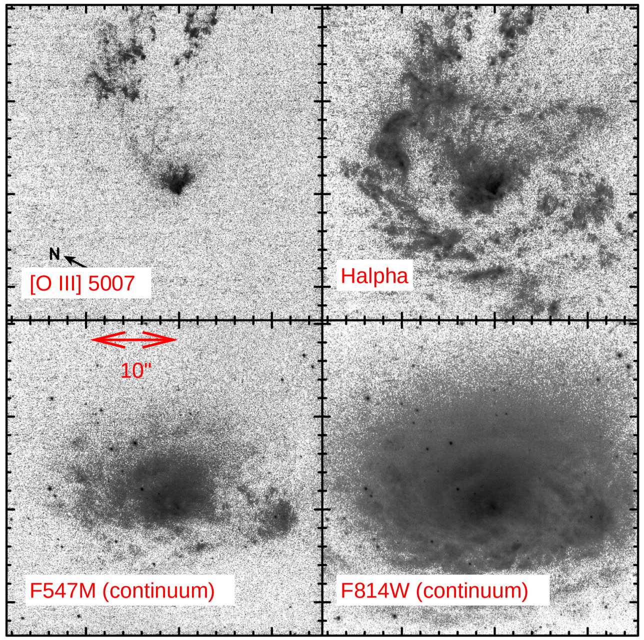

(HST Wilson et al., 2000, Fig. 2)

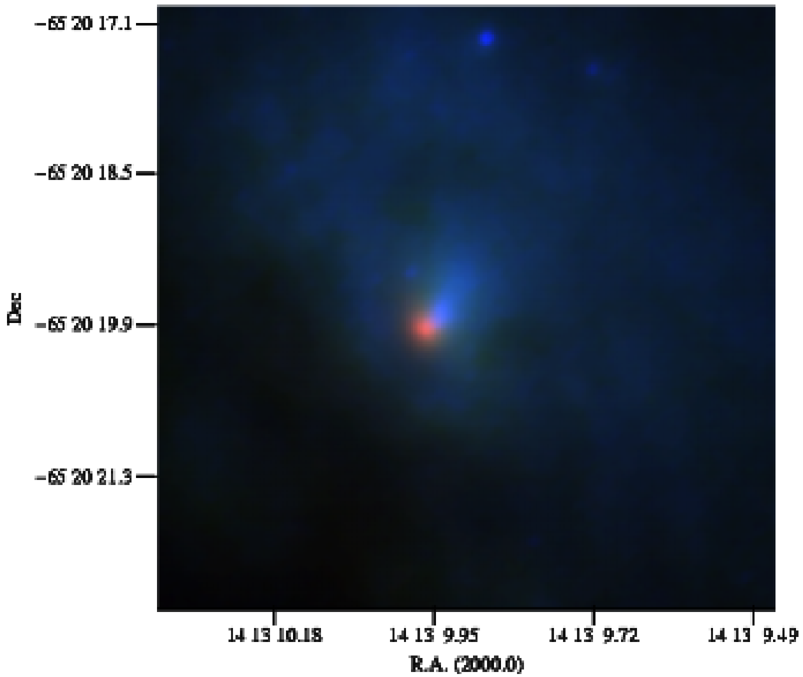

(HST and VLT [IR]; Prieto et al., 2004, Fig. 2)

X-rays (*Chandra*) Optical (HST)

Circinus galaxy: Alignment between hard X-ray emitting gas and optical ionization cone.

Allen, M. G., Dopita, M. A., Tsvetanov, Z. I., & Sutherland, R. S., 1999, ApJ, 511, 686

Baldwin, J. A., Phillips, M. M., & Terlevich, R., 1981, PASP, 93, 5

Kewley, L. J., Groves, B., Kauffmann, G., & Heckman, T., 2006, MNRAS, 372, 961

Komossa, S., & Schulz, H., 1997, A&A, 323, 31

Murayama, T., & Taniguchi, Y., 1998, ApJ, 503, L115

Osterbrock, D. E., 1989, Astrophysics of gaseous nebulae and active galactic nuclei, (Mill Valley, CA: University Science Books)

Osterbrock, D. E., 1991, Rep. Prog. Phys., 54, 579

Pogge, R. W., 1988, ApJ, 328, 519

Prieto, M. A., et al., 2004, ApJ, 614, 135

Wilson, A. S., Shopbell, P. L., Simpson, C., Storchi-Bergmann, T., Barbosa, F. K. B., & Ward, M. J., 2000, AJ, 120, 1325